Journal of
Materials Chemistry C

Materials for optical, magnetic and electronic devices

Accepted Manuscript

This article can be cited before page numbers have been issued, to do this please use: A. L. Mullins, A. iri, I. Zekovic, G. Williams, M. Dramicanin and I. R. Evans, *J. Mater. Chem. C*, 2022, DOI: 10.1039/D2TC02011D.

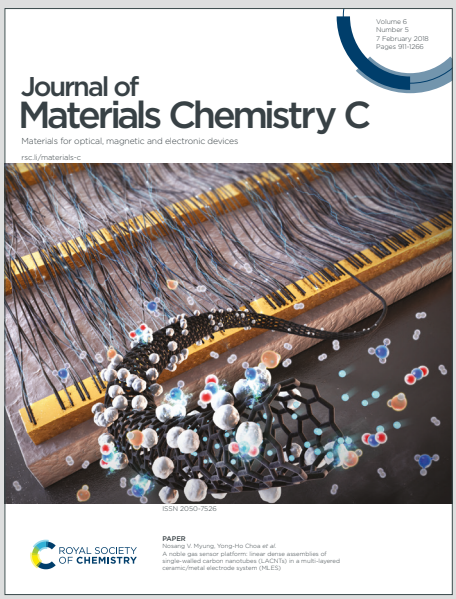

ROYAL SOCIETY OF CHEMISTRY

rsc.li/materials-c

View Article Online
DOI: 10.1039/D2TC02011D

ARTICLE

Received 00th January 20xx,

Accepted 00th January 20xx

DOI: 10.1039/x0xx00000x

Dual-emission luminescence thermometry using $LaGaO_3:Cr^{3+}$, Nd^{3+} phosphors

*Abbi L. Mullins[a], Aleksandar Ćirić[b], Ivana Zeković[b], J. A. Gareth Williams[a], Miroslav D. Dramićanin[b]*and Ivana Radosavljević Evans[a]**

A series of $La_{1-x}Ga_{0.99}O_3$: $Cr_{0.01}$, Nd_x phosphors (where x = 0.005, 0.01, 0.02) for luminescence thermometry was synthesised by the solid-state method, structurally characterised using powder X-ray diffraction data, and investigated by ambient and variable-temperature optical measurements. The design principle relies on the use of a combination of transition metal and rare earth activator ions such that the excitation and emission wavelengths fall within the near infra-red spectral region, notably in the 'first biological window' that is attractive for potential *in vivo* applications. The photoluminescence spectra of the compounds feature the characteristic ^2E phosphorescence of Cr^{3+} at 729 nm and the $^4F_{3/2} \rightarrow {}^4I_{9/2}$ emission of Nd^{3+} around 890 nm. The Nd^{3+} emission is quenched at a higher rate than that of Cr^{3+} with increasing temperature. Thermometric analysis by monitoring the luminescence intensity ratio (LIR) between the emissions of Cr^{3+} and Nd^{3+} from 300 K to 650 K shows a quasi-Boltzmann trend, with a maximum relative sensitivity of ~ 2% K^{-1}, high absolute sensitivity values over this entire temperature range, excellent temperature resolution of 0.04 K at room temperature, and high stability.

1. Introduction

The development of novel ways to accurately monitor small temperature changes is important in numerous applications, including in biomedical systems. Luminescence thermometry is a non-contact method for monitoring temperature changes through their effect on the light-emitting properties of a material, for example, on the intensity of the emission, its decay time, or the profile of the spectrum.[1–3] The use of a luminescence intensity ratio (LIR) method is particularly attractive. Here, the ratio of emission at two distinct wavelengths is monitored, rendering the system self-referencing and less dependent on fluctuations in the efficiency of delivery and collection of light.[4] This approach can allow temperature measurements to be recorded with high accuracy and sensitivity. Most commonly, LIR is observed in systems that can emit from two thermally coupled excited states, according to the following equation:[5,6]

$$LIR(T) = \frac{I_H(T)}{I_L(T)} = B \cdot \exp(-\Delta E / k_B T) \quad (1)$$

where I_H and I_L are the intensities of the higher- and lower-energy excited states, B is a pre-exponential factor, ΔE is the energy difference between the thermally coupled states, k_B = 0.695 cm^{-1} K^{-1} is the Boltzmann constant, and T is the temperature in K. The phosphorescence of one or more activator metal ions doped into a suitable host material offers a potential for luminescence thermometry using such a strategy. Selection of the host material for a solid-state phosphor is critical in providing both stability and control over many of the luminescence properties of the activators.[7] Perovskite-type lanthanum gallate ($LaGaO_3$) has been studied for potential applications in fuel cells, solar cells, and light-emitting displays, amongst others.[8–10] Several $LaGaO_3$-based materials have been reported as hosts for LIR luminescence thermometers that exploit either single or dual emissions from activator ions. For example, $LaGaO_3:Cr^{3+}$ was shown by Mondal *et al.* to have a relative sensitivity of 2.07% K^{-1} at 150 K.[11] Back *et al.* demonstrated that $LaGaO_3:Nd^{3+}$ – which has a distinct temperature marker at 417 K corresponding to the structural phase transition from orthorhombic to rhombohedral – showed a relative sensitivity of 1.59% K^{-1} at 300 K.[12] Meanwhile, materials of composition $LaGaO_3:V^{n+}$, Nd^{3+} were reported by Kniec *et al.* to offer relative sensitivities of 1.0% K^{-1} at 268 and 363 K, 0.49% K^{-1} at 253 K, and 1.44% K^{-1} at 348 K for the V^{5+}, V^{4+}, and V^{3+} doped samples respectively.[13] Most recently, Li *et al.* reported Sm^{3+}, Mn^{4+}-doped LGO phosphors with a maximum relative sensitivity of 2.09% K^{-1} at 456 K.[14] Our own recent work has shown that deconvolution of the overlapped temperature-invariant sharp ^2E emission from the temperature-dependent broadband $^4T_2$ emission of Cr^{3+} in $LaGaO_3$ gives a relative sensitivity of ~2.50% K^{-1} at 300 K and as good temperature resolution as 0.05 K.[15]

a. Department of Chemistry, Durham University, Durham DH1 3LE, UK. E-mail: ivana.radosavljevic@durham.ac.uk
b. Centre of Excellence for Photoconversion, Vinča Institute of Nuclear Sciences – National Institute of the Republic of Serbia, University of Belgrade, P.O. Box 522, Belgrade 11001, Serbia. E-mail: dramican@gmail.com

Lanthanide ions (Ln^{3+}) are in some respects well-suited to luminescence thermometry, owing to their narrow-band emission.[16–21] However, the requirement for thermally coupled excited states restricts the choice of Ln^{3+} dopant.[4] Moreover, Ln^{3+} ions suffer from low absorption coefficients such that the population of their excited states by light absorption is inefficient. Transition metal ions typically have broader absorptions and, usually, higher extinction coefficients, reflecting the greater extent to which the Laporte selection rule is relaxed for *d-d* as opposed to *f-f* transitions. LIR thermometers based on Cr^{3+}, Mn^{4+}, and Ni^{2+} have been investigated, both as single and dual-doped systems.[11,22,23,24,25] The Boltzmann equilibrium between the closely separated ^2E and $^4T_2$ excited states of d^3 ions such as Cr^{3+} underpins them.[26–29]

The aim of the present study was to combine the complementary advantages of lanthanide and transition metal ions in the design of a luminescent thermometer that would function in the near-infrared (NIR) region. The neodymium(III) ion was selected for investigation with Cr^{3+}, as Nd^{3+} not only emits in the NIR but also has a number of excited states of energies that overlap with the emission of Cr^{3+}, allowing for Cr^{3+}-to-Nd^{3+} energy transfer.[10] The narrow-band nature of the ^2E emission of Cr^{3+}, as well as that of the lanthanide ion, and their separation of >200 nm ensures good discrimination for luminescence thermometry readout. The characteristic Nd^{3+} line emissions fall into the part of the NIR region known as the 'first biological window' (biological tissue being relatively transparent to this part of the spectrum), allowing for potential applications in biomedical imaging, including *in vivo* temperature sensing.[30] Marciniak *et al.* have reported phosphors utilising the Cr^{3+}, Nd^{3+} combination; for example, the material $LiLaP_4O_{12}$:$Cr^{3+}_{0.01}$, $Nd^{3+}_{0.10}$ shows thermometric properties in the physiological temperature range with a relative sensitivity of 4.89 % K^{-1} at 323K. [31,32] Here, we report the solid-state synthesis, structural characterisation, and photoluminescence (PL) properties of a series of Cr^{3+} and Nd^{3+}-doped LGO phosphors. Variable-temperature photo-luminescence measurements were performed to investigate the excitation, emission, and energy transfer of the system. Extensive thermometric analysis – including sensitivities, temperature resolution and repeatability – was undertaken to characterise the luminescent thermometry performance.

2. Experimental Methods

2.1 Synthesis

All samples were synthesised by conventional solid-state reaction methods from stoichiometric quantities of reactants to prepare 2 g of product.[12] La_2O_3 powder (Aldrich, ≥ 99.99%) was pre-heated to 900°C for 10 h to remove moisture. The pre-dried La_2O_3, Ga_2O_3 (Aldrich, ≥ 99.99%), Cr_2O_3 (Aldrich, 99.9%), and Nd_2O_3 (Aldrich, 99.9%) powders were ground for approximately 30 min with an agate mortar and pestle, pressed into 10 mm pellets, and placed into alumina crucibles with lids. Samples were sintered in a muffle furnace at 1200°C in air for 60–100 h with intermittent grinding.

2.2 Powder X-ray Diffraction (PXRD)

PXRD was used to monitor the progress of the reactions and to determine the purity of the products. All measurements were carried out at room temperature using a Bruker AXS d8 Advance diffractometer utilising CuKα radiation and a Lynx-Eye detector. Patterns were recorded in a range of 10°<2θ<90° with a step size of 0.02° and step time of 0.5 s. All patterns were analysed by Rietveld fitting in TOPAS academic software.[33,34] Refined parameters included background polynomial terms, zero-point, pseudo-Voigt peak shape function terms, unit cell parameters, and an overall isotropic atomic displacement parameter.

2.3 Photoluminescence Spectroscopy

The PL properties of $La_{1-x}Ga_{0.99}O_3$: $Cr_{0.01}$, Nd_x (x = 0.005, 0.01, 0.02) were studied using a Horiba Jobin-Yvon Fluorolog-3 spectrometer. The excitation source was a 450W xenon lamp. The emitted light was detected using either a red-sensitive photomultiplier tube (Hamamatsu R928) or a CCD detector (Horiba Synapse back-illuminated deep depletion) offering good sensitivity up to 1000 nm. NIR emission at λ > 1000 nm was monitored using a Hamamatsu NIR photomultiplier tube. Samples were analysed either in 3 mm o.d. quartz capillary tubes within the instrument's sample compartment, or externally using a Quanta-phi integrating sphere coupled to the instrument with optical fibres. Long-pass 400 nm and 850 nm filters were utilised to remove harmonic peaks in RT excitation and emission spectra. Lifetime data were acquired using an Edinburgh Instruments OB920 following excitation of the samples in 3 mm o.d. quartz capillaries with a microsecond-pulsed flashlamp. Emitted light was detected at right angles using an R928 detector operating in multichannel scaling mode. The variation in PL intensity with temperature over the range 300 – 650 K was investigated for all Cr^{3+}, Nd^{3+} doped compounds using an Ocean Insight FX spectrometer with bifurcated fibre-optics and a custom-built thermometry apparatus.[35] Samples were excited at 473 nm using a 150 mW high-stability laser.

3. Results and Discussion

3.1 Structural characterisation

All PXRD patterns were fitted using orthorhombic $LaGaO_3$ as the initial structural model.[36] Fig. 1 shows the final Rietveld fits obtained and Table 1 summarises main crystallographic parameters.

DOI: 10.1039/D2TC02011D

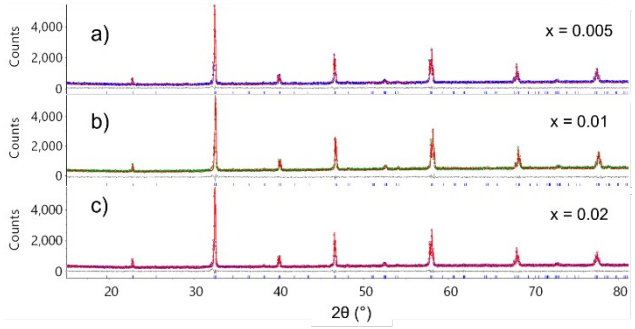

Figure 1: Rietveld fits of the XRD data collected on $La_{1-x}Ga_{0.99}O_3$: $Cr_{0.01}$, Nd_x – a) x = 0.005, b) x = 0.01, and c) x = 0.02 samples. In each case the red curve represents the calculated pattern; the green, purple, and blue represents the observed data, whilst the difference curve is depicted in grey.

Fig. 2 shows the perovskite-type structure of $LaGaO_3$, made up of a network of corner-sharing GaO_6 octahedra with interspersed La^{3+} ions. Having a Goldschmidt tolerance factor t = 0.973, $LaGaO_3$ is orthorhombic, crystallising in space group *Pnma* (no. 62). The departure from the cubic symmetry is due to the tilting of the GaO_6 octahedra – in Glazer notation, from $a^0a^0a^0$ to $a^+b^-b^-/a^+a^-a^-$ - resulting in the change of the La^{3+} environment and a lowering of the La^{3+} coordination number (CN) from 12 to 8.[37] In space group *Pnma*, La^{3+} and Ga^{3+} are located on Wyckoff sites 4c and 4a, with site symmetry m and $\bar{1}$, respectively. Given the ionic radii of the species involved, it can be expected that Nd^{3+} (1.109 Å, CN = 8) will readily substitute for La^{3+} (1.160 Å, CN = 8), and that Cr^{3+} (0.615 Å, CN = 6) will substitute for Ga^{3+} (0.620 Å, CN = 6).[38]

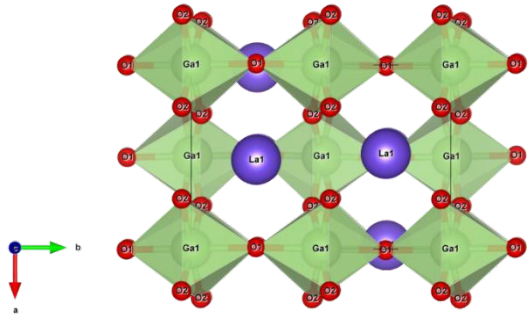

Figure 2: Unit cell of $LaGaO_3$: $Cr_{0.01}$, $Nd_{0.02}$ viewed down the crystallographic c-axis. La^{3+} is shown in purple, Ga^{3+} in green, and O^{2-} in red.

3.2 Room temperature photoluminescence analysis

The emission spectra of all three samples upon the excitation at 590 nm (*i.e.*, in the region of the spin-allowed $^4A_{2g} \rightarrow {}^4T_{2g}$ absorption of Cr^{3+}) show two well-defined sets of bands: one set in the 700–750 nm region attributable to the ^2E emission of Cr^{3+} and the other in the 860–930 nm range due to the $^4F_{3/2} \rightarrow {}^4I_{9/2}$ transitions of the Nd^{3+} ion (Fig. 3c). The absence of broadband fluorescence corresponding to the strongly field-dependent, spin-allowed $^4T_{2g}$ to $^4A_{2g}$ transition of Cr^{3+} indicates that the Cr^{3+} ions in the CrO_6 octahedra experience a strong-field local environment, such that the $^4T_{2g}$ state lies at significantly higher energy than the ^2E. The peak at 739 nm for all three samples is indicative of an exchange-coupled Cr^{3+}-Cr^{3+} pair N-line.[39,40] The contribution of the N-line to the spectrum should be concentration-dependent but, as all three samples contain 1.0% Cr^{3+}, the N-line peaks are of approximately equal relative intensity in this instance. Stokes and anti-Stokes sidebands are seen for each sample on either side of the ^2E R-line emission.[41]

The distinct line-like emission of the Nd^{3+} $^4F_{3/2} \rightarrow {}^4I_{9/2}$ transition centred at about 890 nm increases with increasing Nd^{3+} concentration relative to the Cr^{3+} ^2E emission (Fig. 3c). As the Nd^{3+} concentration increases, there is also evidence of an increasing contribution from the $^4F_{5/2} \rightarrow {}^4I_{9/2}$ transition at around 800 nm (Fig. 3c). The $^4F_{5/2}$ excited state is thermally coupled to the $^4F_{3/2}$ at room temperature due to the small difference in energy between them.[42] Fig. 3d gives the NIR emission spectrum of the samples, showing the $^4F_{3/2}$ to $^4I_{11/2}$

Table 1: Refined unit cell parameters for the $La_{1-x}Ga_{0.99}O_3$: $Cr_{0.01}$, Nd_x (x = 0.005, 0.01, 0.02) series.

Sample	R_{wp} (%)	a (Å)	b (Å)	c (Å)	Cell Volume (Å^3)
$La_{0.995}Nd_{0.005}Ga_{0.99}Cr_{0.01}O_3$	5.52	5.4924(1)	7.7747(1)	5.5241(1)	235.895(8)
$La_{0.99}Nd_{0.01}Ga_{0.99}Cr_{0.01}O_3$	5.35	5.49259(9)	7.7745(1)	5.52399(9)	235.890(7)
$La_{0.98}Nd_{0.02}Ga_{0.99}Cr_{0.01}O_3$	5.75	5.4923(1)	7.7745(1)	5.5227(1)	235.828(8)

View Article Online
DOI: 10.1039/D2TC02011D

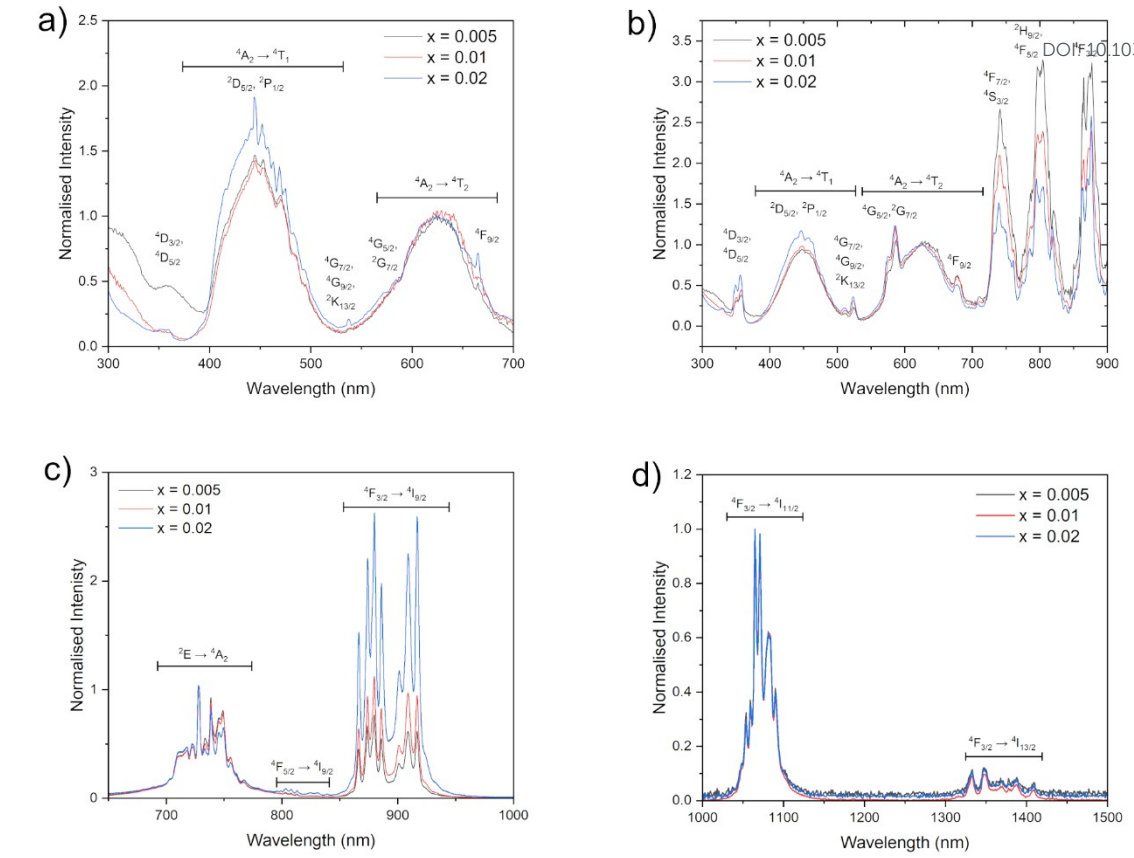

Figure 3: Normalised spectra of La1-xGaO$_3$:Cr$_{0.01}$, Nd$_x$ a) Excitation spectra of Cr^{3+} monitored at λ_{em} = 729 nm, normalised at 622 nm; b) Excitation spectra of Nd^{3+} monitored at λ_{em} = 1071 nm, normalised at 622 nm; c) Normalised emission spectra of the three members of the LaGaO$_3$: Cr, Nd series normalised at 729 nm, λ_{ex} = 590 nm;, d) Emission spectra in the NIR region > 1000 nm, λ_{ex} = 590 nm.

emission centred at 1070 nm, and $^4F_{3/2}$ to $^4I_{11/2}$ emission centred at 1360 nm. The observed Nd^{3+} emissions could arise, at least in part, from direct excitation of the $^4I_{9/2} \rightarrow {}^4G_{5/2}$ transition at the excitation wavelength used, although the $^4F_{5/2}$ state could also be populated indirectly by energy transfer from Cr^{3+}, given the overlap of the Cr^{3+} ^2E emission with excitations of Nd^{3+} to the $^4F_{7/2}$, $^4S_{3/2}$, and $^4F_{9/2}$ states.

Excitation spectra can help to determine whether or not such energy transfer is significant. The excitation spectra of the samples monitored for the Cr^{3+} ^2E emission at 729 nm and for the $^4F_{3/2} \rightarrow {}^4I_{9/2}$ of Nd^{3+} at 905 nm are shown in Figs. 3a and 3b, respectively. The Cr^{3+} excitation spectrum shows two broad bands at 624 and 444 nm attributed to the Cr^{3+} $^4A_{2g} \rightarrow {}^4T_{2g}$ and $^4A_{2g} \rightarrow {}^4T_{1g}$ transitions, respectively. There is also some evidence of sharper line-like excitations at 665, 584, 537, 444, and 354 nm, superimposed on the broad Cr^{3+} bands, most evident for the *x* = 0.02 sample with the highest Nd^{3+} concentration. The wavelengths of these peaks correspond well to the energies of the $^4F_{9/2}$; $^4G_{5/2}$ and $^2G_{7/2}$; $^4G_{7/2}$, $^4G_{9/2}$ and $^2K_{13/2}$; $^2D_{5/2}$ and $^2P_{1/2}$; and $^4D_{3/2}$ and $^4D_{5/2}$ excited states of Nd^{3+}. Their appearance in the excitation spectrum of the Cr^{3+} ions suggests that some $Nd^{3+} \rightarrow Cr^{3+}$ energy transfer is occurring. The Nd^{3+} excitation spectrum, Fig. 3b, shows sharp peaks for excitation to the $^4F_{3/2}$ at 880 nm; $^2H_{9/2}$ and $^4F_{5/2}$ at 810 nm; $^4F_{7/2}$ and $^4S_{3/2}$ at 740 nm; $^4F_{9/2}$ at 680 nm; $^4G_{5/2}$ and $^2G_{7/2}$ at 590 nm; $^4G_{7/2}$, $^2G_{9/2}$, and $^2K_{13/2}$ at 520 nm; $^2D_{5/2}$, and $^2P_{1/2}$ at 440 nm; and $^4D_{3/2}$, and $^4D_{5/2}$ states at 350 nm. [42] Notably, the excitation spectrum of the Nd^{3+} emission does also prominently feature the broad bands associated with Cr^{3+}, suggesting that some $Cr^{3+} \rightarrow Nd^{3+}$ energy transfer is occurring for these materials at room temperature. Energy transfer between activator ions is illustrated schematically in Fig. 4 showing the relative energies of pertinent states on Cr^{3+} and Nd^{3+}. The decline in the relative intensity of the Nd^{3+} relative to the Cr^{3+} excitations with

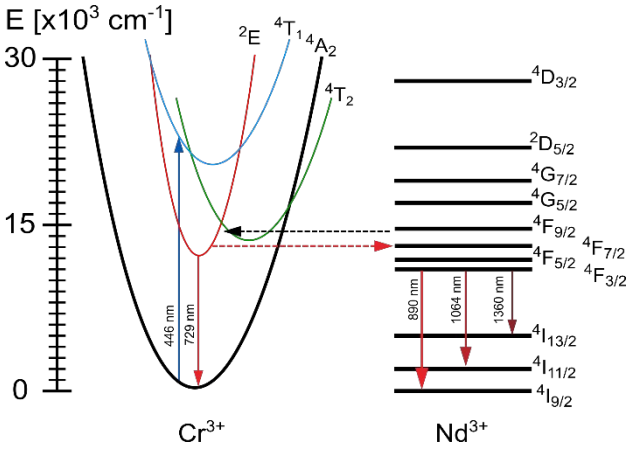

Figure 4: Energy level diagram showing energy transfer between Cr^{3+} and Nd^{3+} ions, with filled straight lines showing emission/excitation, and dashed lines denoting energy transfer from Cr^{3+} to Nd^{3+} in red, and Nd^{3+} to Cr^{3+} in black, respectively.

View Article Online
DOI: 10.1039/D2TC02011D

increasing Nd^{3+} content may be indicative of a degree of quenching between Nd^{3+} ions.

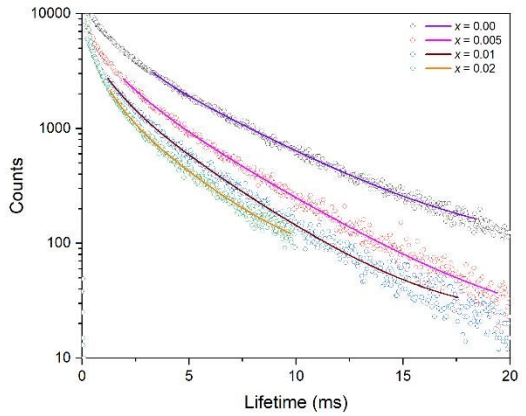

Figure 5: Lifetime data (circles) and bi-exponential fits (lines) of $LaGaO_3:Cr_{0.01}$ (x = 0.00) and of $La_{1-x}Ga_{0.99}O_3$: $Cr_{0.01}$, Nd_x (x = 0.005, 0.01, and 0.02).

The lifetimes of the Cr^{3+} emission at 729 nm were measured for $LaGa_{0.99}O_3:Cr_{0.01}$ and the Nd^{3+}-doped samples at room temperature, Fig. 5. The data fitted well to a bi-exponential decay with a *y* offset for dark-count, giving an average lifetime of 4.2 ms for the -Cr^{3+}-only sample, compared to values of 3.6, 3.0, and 2.5 ms for the x = 0.005, 0.01 and 0.02 samples. The trend of decreasing lifetime of the Cr^{3+} ^2E state with increasing Nd^{3+} doping supports the conclusion above that $Cr^{3+} \rightarrow Nd^{3+}$ energy transfer is occurring. The energy transfer efficiency, η_{ET}, was calculated to be 14%, 28%, and 40% respectively using equation (2), where τ_{Cr} is the lifetime of the chromium-only sample and $\tau_{Cr\text{-}Nd}$ that of the dual-doped sample.[43]

$$\eta_{ET} = 1 - \frac{\tau_{Cr-Nd}}{\tau_{Cr}} \qquad (2)$$

3.3 Luminescence thermometry

Temperature-dependent spectra of $La_{1-x}Ga_{0.99}O_3$: $Cr_{0.01}$, Nd_x phosphors (where x = 0.005, 0.01, 0.02) are presented in Figs. 6a-c. As sample $La_{0.98}Ga_{0.99}O_3$: $Cr_{0.01}$, $Nd_{0.02}$ showed comparable intensities from the Cr^{3+} and Nd^{3+} ions, it was selected for thermometric evaluation. The 808 nm emission band of Nd^{3+} overlaps with the tail of the broad emission from the $^4T_2$ level of Cr^{3+} and was therefore excluded from the analysis. The pure Cr^{3+} and Nd^{3+} emissions are considered at λ < 790 nm (N-lines, ^2E) and λ > 850 nm, respectively. The Cr^{3+} emission experiences simultaneous increase of emissions from the $^4T_2$ level and decrease of intensity of emissions from ^2E level and N-lines with increasing temperature, such that the overall Cr^{3+} emission intensity is quenched more slowly than the $^4F_{3/2} \rightarrow {}^4I_{9/2}$ emission of Nd^{3+}. The intensities were fitted to Eq. 1, where $I_H = I(Cr^{3+})$, and $I_L = I(Nd^{3+})$, and the resultant LIR is presented in Fig. 6d. The energy gap used in Eq. 1 does not represent the gap between the thermalised levels, but instead the two emission centres – the Cr^{3+} and Nd^{3+} activator ions. The quasi-Boltzmann relation to which the experimental data are fitted is given by:

$$LIR = \frac{I(\mathrm{Cr}^{3+})}{I(\mathrm{Nd}^{3+})} = 63.9(8)\exp\left(\frac{1170(59)}{k_B T}\right) \qquad (3)$$

with a high quality of fit of adj. R^2 = 0.997. The fitted energy gap is larger than that between the thermalised levels of all the lanthanides but Eu^{3+}, meaning that the relative sensitivity will have a relatively high value. The high value of the temperature-invariant parameter B in Eq. 1 is an indication of the high absolute sensitivity of this probe. The absolute and relative sensitivities respectively (Fig. 5e) were obtained by:

$$S_a[K^{-1}] = \left|\frac{\partial LIR}{\partial T}\right| = \frac{\Delta E}{k_B T^2} B \exp\left(-\frac{\Delta E}{k_B T}\right) \qquad (4)$$

$$S_r[\%\, K^{-1}] = \frac{S_a}{LIR} 100\% = \frac{\Delta E}{k_B T^2} 100\% \qquad (5)$$

The relative sensitivity, S_r, was calculated as ~2.0% K^{-1} at 300K, which is, as predicted, a value higher than achieved with most of the lanthanides (see Table 2 in Ref. 4)

The sensor stability was tested and confirmed by estimating LIR while cycling between two temperatures in 10 periods (see Fig. 5f). The LIR values at those temperatures remained unchanged after each cycle. The repeatability was estimated according to:[44]

$$R[\%] = \left(1 - \frac{\max(|\mathrm{mean(LIR)} - \mathrm{LIR}_i|)}{\mathrm{mean(LIR)}}\right) \cdot 100\% \qquad (6)$$

where i denotes the measurement count. For the measurements presented in Fig. 5f, the repeatability is 99.92% and 99.88% at 350 K and 500 K, respectively.

Finally, the relative uncertainties (σ_r) were estimated from 30 consecutive measurements at 300 K and 435 K, with values of 0.07% and 0.09%, respectively (see Fig. 5g,h). Corresponding temperature resolutions of 0.04 K and 0.1 K were estimated using equation (7).

$$\Delta T = \frac{\sigma_r}{S_r} \qquad (7)$$

Although our material does not exhibit the same sensitivity as some other Cr^{3+}, Nd^{3+} - containing luminescence thermometers in the literature, it provides high precision and therefore excellent temperature resolution. The reason behind the low uncertainties in temperature measurements using this probe is that both emissions utilised for LIR have high intensities. Swieten at al.[45] recently demonstrated that signal strength is directly proportional to the precision of the temperature measurement. As already mentioned, Cr^{3+} emission in the strong crystal field is comprised of the $^4T_2$ and ^2E bands, with opposite trends with change in temperature. These bands overlap, but as the $^4T_2$ band is broader, there is always a spectral region which comprises only of the $^4T_2$ band. The emission of the entire Cr^{3+} emission, comprised of $^4T_2$ and ^2E bands, changes more slowly with temperature than each individual band. By taking a narrow spectral range for LIR, containing only $^4T_2$ emission, the larger uncertainty is introduced than by observing

View Article Online
DOI: 10.1039/D2TC02011D

the entire Cr^{3+} emission as it is obvious that the entire emission is more intense than any of its individual parts. Thus, the higher sensitivity that can be obtained by employing only $^4T_2$ emission in LIR does not necessarily mean that the temperature resolution is improved, as the increased relative sensitivity can be compensated by the increased uncertainty. The analogous demonstration is presented in our previous work where we showed that by deconvolution of $^4T_2$ and ^2E bands the relative sensitivity can be significantly increased, but the temperature resolution stays invariant to the numerical method employed for LIR.[46] In a YAG matrix, a high temperature sensitivity of 3.48% K^{-1} was observed, but only a fraction of Cr^{3+} emission was employed for the integration used for the LIR calculation.[47] In a Cr^{3+}, Nd^{3+} doped $Y_3Al_2Ga_3O_{12}$ host, a relative sensitivity of 2.2% K^{-1} was observed with even narrower integrated areas.[48] An investigation of $Gd_3Ga_5O_{12}$ gave a relative sensitivity of 1.90% K^{-1} by LIR, using only the ratio of the broad-band of Cr^{3+} divided to the Nd^{3+} emission.[24] An outstanding relative sensitivity of 4.89% K^{-1} was reported for a Cr^{3+}, Nd^{3+} co-doped system in $LiLaP_4O_{12}$ host, but using 20 nm-wide integration windows for both Cr^{3+} and Nd^{3+}, and with high emission intensities only at lower temperatures.[32] Thus, in Cr^{3+}, Nd^{3+} co-doped systems, the sensitivity of LIR requires a compromise between the precision of the measurement and the sensitivity. A robust comparison of the most important figure of merit in thermometry – the temperature resolution – in different materials would necessitate measuring all the materials under the same experimental conditions. For comparison of the most prominent and highly performing probes for luminescence thermometry by the LIR method with our sensor please see Table 2.

View Article Online
DOI: 10.1039/D2TC02011D

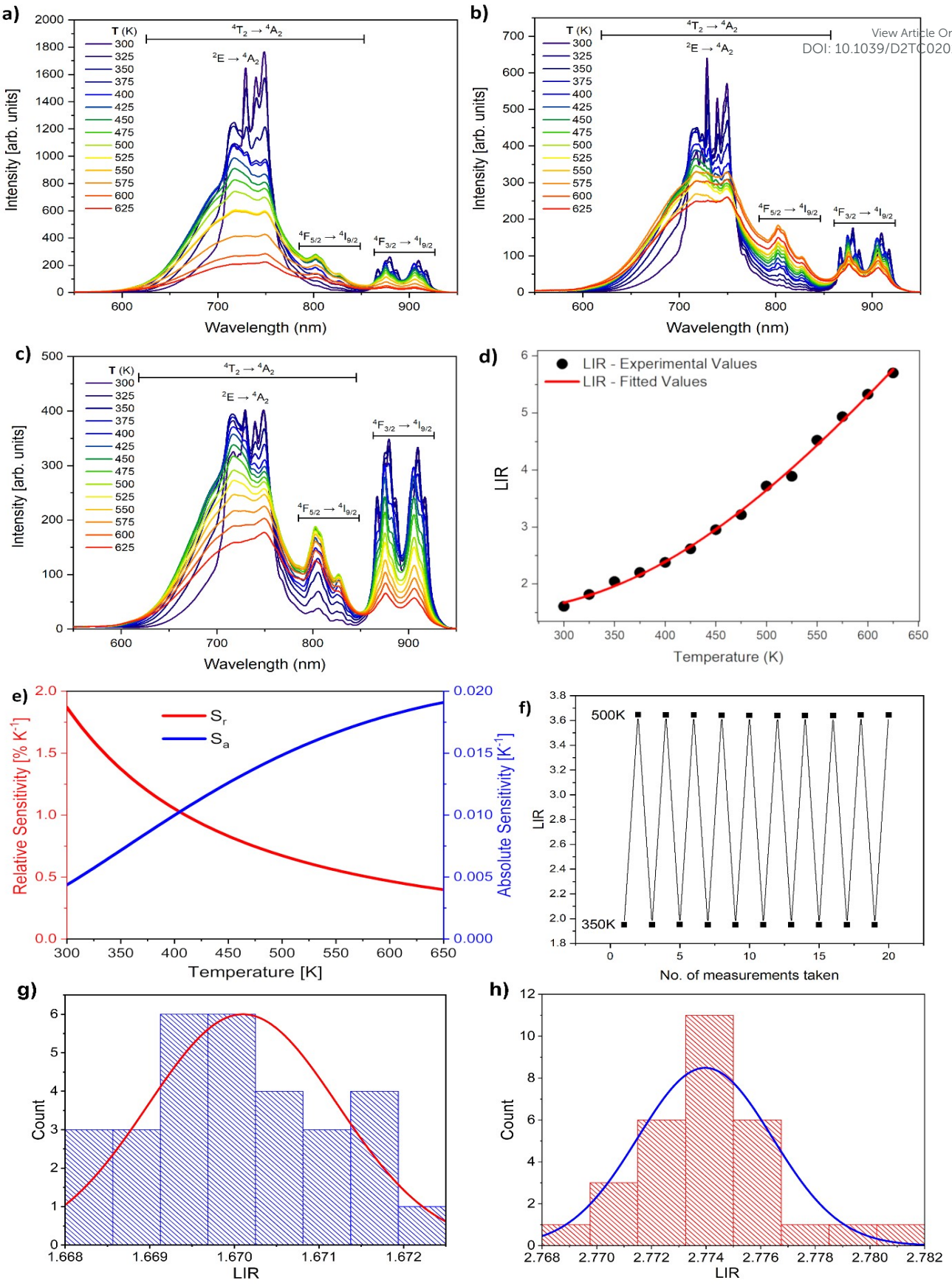

Figure 6: Emission spectra of a) Nd^{3+} x = 0.005 sample, b) x = 0.01, and c) Nd^{3+} x = 0.02 all excited at 473 nm. d) Fitted LIR of the x = 0.02 sample. e) Absolute (red) and relative (black) sensitivities of the x = 0.02 sample. f) Repeatability of the x = 0.02 sample's LIR by cycling between 350 and 500 K. Distribution curve of LIR after 30 consecutive measurements at g) 300 K, and h) 435 K.

View Article Online
DOI: 10.1039/D2TC02011D

ARTICLE

Table 2. Comparison of thermometric performance of Cr^{3+} or Nd^{3+} doped LGO, Cr^{3+},Nd^{3+} co-doped systems, or other prominent probes with LGO:Cr^{3+},Nd^{3+}, by the LIR method.

Host	Activator	T range [K]	S_r [% K^{-1}] @ 310 K	Max(S_r) [% K^{-1}]	S_a [K^{-1}] @ 310 K	ΔT [K] @ 310 K	Min(ΔT) [K]	Ref.
ZnS	Mn^{2+},Eu^{3+}	303-423	NA	1.1 @303 K	NA	NA	0.02	49
YF_3	Er^{3+},Yb^{3+}	293-473	1.8	2 @ 293 K	4.2×10^{-3}	1.1	1	50
ZnSe/CdSe	Mn^{2+}	200-370	1.2	1.2 @ 310 K	NA	NA	NA	51
$MgAl_2O_4$	Cr^{3+}	300-540	3.4	3.5 @ 300 K	4.0×10^{-3}	0.3	0.3	52
$ZnGa_2O_4$	Cr^{3+}	300-700	2.8	3.2 @ 300 K	1.4×10^{-3}	0.4	0.4	53
$Bi_2Ga_4O_9$	Cr^{3+}	150-450	0.7	0.75 @ 300 K	NA	1.5	1.5	54
$Sr_2MgAl_{22}O_{36}$	Cr^{3+}	298-523	1.7	2 @ 300 K	4.5×10^{-1}	NA	NA	55
YVO_4	Eu^{3+}	300-850	3.9	4.2 @ 300 K	5.8×10^{-7}	NA	NA	56
La_2O_3	Yb^{3+},Nd^{3+}	290-1230	2.9	3 @ 300 K	1.4×10^{-4}	0.7	0.6	57
Al_2O_3	Sm^{2+}	298-648	4.7	4.8 @ 298 K	3.3×10^{-3}	0.04	0.04	58
YAB	Pr^{3+},Gd^{3+}	30-800	0.8	10 @ 30 K	NA	0.6	0.6	59
$LiLuF_4$	Er^{3+},Yb^{3+}	300-525	1.2	1.3 @ 300 K	NA	0.09	0.08	60
$NaYF_4$	Er^{3+},Yb^{3+}	300-900	1.1	1.1 @ 300 K	3.6×10^{-3}	1	1	61
Ga_2S_3:La_2O_3	Er^{3+},Yb^{3+}	293-493	1.0	1.1 @ 293 K	NA	0.3	0.3	62
LGO	Cr^{3+}	150-300	0.7	2.07 @ 150 K	1.9×10^{-2}	0.7	0.2	11
LGO	Nd^{3+}	280-830	1.5	1.8 @ 280 K	NA	1.2	1.6	12
LGO	V^{n+},Nd^{3+}	123-573	1.0	1.5 @ 350 K	NA	NA	NA	13
LGO	Cr^{3+}	300-600	2.4	2.5 @ 300 K	NA	0.05	0.05	15
$Gd_3Al_5GaO_{12}$	Cr^{3+},Nd^{3+}	123-573	1.2	1.9 @ 123 K	NA	NA	NA	24
$LaScO_3$	Cr^{3+},Nd^{3+}	123-573	0.2	1.3 @ 400 K	NA	NA	NA	25
$LiLaP_4O_{12}$	Cr^{3+},Nd^{3+}	113-473	3.6	3.9 @ 323 K	NA	NA	NA	31
$LiLaP_4O_{12}$	Cr^{3+},Nd^{3+}	300-420	NA	4.9 @ 323 K	NA	NA	0.05	32
YAG	Cr^{3+},Nd^{3+}	100-850	3.3	3.5 @ 200 K	NA	NA	NA	47
YAGG	Cr^{3+},Nd^{3+}	123-573	1.1	2.16 @ 220 K	NA	NA	NA	48
LGO	Cr^{3+},Nd^{3+}	300-625	1.8	1.9 @ 300 K	4.9×10^{-3}	0.04	0.04	This work

Conclusions

Phosphors of composition $La_{1-x}Ga_{0.99}O_3$: $Cr_{0.01}$, Nd_x (x = 0.005, 0.01, 0.02) were successfully synthesised by the solid-state method and structurally characterised by PXRD using Rietveld refinement. The excitation into the spin-allowed absorption bands of Cr^{3+} at 590 nm gives rise to both the narrow-band, spin-forbidden ^2E emission of Cr^{3+} at 729 nm and the $^4F_{3/2} \rightarrow {}^4I_{9/2}$ line-like emissions of Nd^{3+} at around 890 nm. At room temperature, energy transfer both from $Cr^{3+} \rightarrow Nd^{3+}$ and from $Nd^{3+} \rightarrow Cr^{3+}$ was evident by examination of excitation spectra registered at the well-separated Nd^{3+} and Cr^{3+} emission wavelengths.

It is demonstrated that $La_{0.98}Ga_{0.99}O_3$: $Cr_{0.01}$, $Nd_{0.02}$ can be used as an efficient NIR thermometer. This binary probe follows the Boltzmann relation, with good sensitivity values. Due to the high intensities of both the Nd^{3+} and Cr^{3+} emissions, the absolute sensitivity has high values (S_r ~2.0% K^{-1} at 300 K) and the uncertainties in measurement are low, leading to an excellent temperature resolution (0.04 K at 300 K), even for inexpensive non-state-of-the-art equipment. Demonstrating this low uncertainty, and therefore high temperature resolution, whilst employing instrumentation that is closer to that utilised in industry, gives this probe the unique advantage of authenticity in testing for potential real-world applications. The sensor also shows potential to be used for temperature measurements of biological samples *in vivo*, as both the excitation and emission can be reached within the first biological window.

Conflicts of interest

There are no conflicts to declare.

View Article Online
DOI: 10.1039/D2TC02011D

Acknowledgements

The authors acknowledge funding by NATO grant SPS.MYP G5751 (The Optical Nose Grid for Large Indoor Area Explosives Vapours Monitoring) and from the Ministry of Education, Science and Technological Development of the Republic of Serbia. ALM thanks EPSRC for a PhD studentship from the Doctoral Training Programme. We thank Peter Rodger and Gary Oswald for preliminary exploratory synthesis and PXRD data collection during the covid-19 pandemic.

Notes and references

1 C. D. S. Brites, A. Millan and L. D. Carlos, *Lanthanides in luminescent thermometry Handbook on the Physics and Chemistry of Rare Earths*, 2016.
2 C. D. S. Brites, P. P. Lima, N. J. O. Silva, A. Millán, V. S. Amaral, F. Palacio and L. D. Carlos, *Nanoscale*, 2012, **4**, 4799–4829.
3 M. D. Dramićanin, *J. Appl. Phys*, 2020, **128**, 040902.
4 M. D. Dramićanin, *Methods Appl. Fluoresc.*, 2016, **4**, 042001.
5 S. F. Collins, G. W. Baxter, S. A. Wade, T. Sun, K. T. V. Grattan, Z. Y. Zhang and A. W. Palmer, *J. Appl. Phys*, 1998, **84**, 4649–4654.
6 G. (Greg) Baxter, S. Wade, S. Collins, G. Monnom and E. Maurice, *Proceedings of SPIE - The International Society for Optical Engineering*.
7 G. Blasse and B. C. Grabmaier, *Luminescent Materials*, Springer-Verlag, 1994.
8 Ch. S. Kamal, T. K. V. Rao, T. Samuel, P. V. S. S. S. N. Reddy, J. B. Jasinski, Y. Ramakrishna, M. C. Rao and K. R. Rao, *RSC Adv.*, 2017, **7**, 44915–44922.
9 T. Ishihara, H. Matsuda and Y. Takita, *J. Am. Chem. Soc.*, 1994, **116**, 3801–3803.
10 L. Zhang, L. Dong, B. Shao, S. Zhao and H. You, *Dalton Trans.*, 2019, **48**, 11460–11468.
11 A. Mondal and J. Manam, *Ceram. Int.*, 2020, **46**, 23972–23984.
12 M. Back, J. Ueda, J. Xu, D. Murata, M. G. Brik and S. Tanabe, *ACS Appl. Mater. Interfaces*, 2019, **11**, 38937–38945.
13 K. Kniec and L. Marciniak, *Phys. Chem. Chem. Phys.*, 2018, **20**, 21598–21606.
14 Z. Li, X. Yu, T. Wang, S. Wang, L. Guo, Z. Cui, G. Yan, W. Feng, F. Zhao, J. Chen, X. Xu and J. Qiu, *J. Am. Ceram. Soc.*, DOI:10.1111/jace.18286.
15 A. L. Mullins, A. Ćirić, Z. Ristić, J. A. Gareth Williams, I. R. Evans, and M. D. Dramićanin. *J. Lumin.,* 2022*,* **246**, 118847.
16 V. Lojpur, S. Ćulubrk, M. Medić and M. Dramicanin, *J. Lumin* , 2016, **170**, 467–471.
17 S. Ćulubrk, V. Lojpur, S. P. Ahrenkiel, J. M. Nedeljković and M. D. Dramićanin, *J. Lumin* , 2016, **170**, 395–400.
18 Lj. R. Đačanin, S. R. Lukić-Petrović, D. M. Petrović, M. G. Nikolić and M. D. Dramićanin, *J. Lumin* , 2014, **151**, 82–87.
19 S. Balabhadra, M. L. Debasu, C. D. S. Brites, L. A. O. Nunes, O. L. Malta, J. Rocha, M. Bettinelli and L. D. Carlos, *Nanoscale*, 2015, **7**, 17261–17267.
20 V. K. Rai, D. K. Rai and S. B. Rai, *Sens. Actuators A Phys.*, 2006, **128**, 14–17.
21 Y. Shen, X. Wang, H. He, Y. Lin and C.-W. Nan, *Compos Sci Technol*, 2012, **72**, 1008–1011.
22 D. K. Amarasinghe and F. A. Rabuffetti, *Chem. Mater.*, 2019, **31**, 10197–10204.
23 C. Matuszewska, K. Elzbieciak-Piecka and L. Marciniak, *J. Phys. Chem. C*, 2019, **123**, 18646–18653.
24 K. Elzbieciak, A. Bednarkiewicz and L. Marciniak, *Sens. Actuators B Chem.*, 2018, 96–102.
25 K. Elzbieciak-Piecka, M. Suta and L. Marciniak, *Chem. Eng. J.*, 2021, **421**, 129757.
26 A. Ćirić, Z. Ristić, J. Periša, Ž. Antić and M. D. Dramićanin, *Ceram.*, 2021, **47**, 27151–27156.
27 Z. Ristić, V. Đorđević, M. Medić, S. Kuzman, M. Sekulić, Ž. Antić and M. D. Dramićanin, *Meas. Sci. Technol.*, 2021, **32**, 054004.
28 M. Back, E. Trave, J. Ueda and S. Tanabe, *Chem. Mater.*, 2016, **28**, 8347–8356.
29 E. Glais, M. Pellerin, V. Castaing, D. Alloyeau, N. Touati, B. Viana and C. Chanéac, *RSC Adv.*, 2018, **8**, 41767–41774.
30 A. N. Bashkatov, E. A. Genina, V. I. Kochubey and V. V. Tuchin, *J. Phys. D*, 2005, **38**, 2543–2555.
31 L. Marciniak, A. Bednarkiewicz, D. Kowalska and W. Strek, *J. Mater. Chem. C*, 2016, **4**, 5559–5563.
32 L. Marciniak, A. Bednarkiewicz and W. Strek, *Sens. Actuators B Chem*, 2017, **238**, 381–386.
33 A. A. Coelho, J. Evans, I. Evans, A. Kern and S. Parsons, *Powder Diffr.*, 2011, **26**, S22–S25.
34 H. M. Rietveld, *J. Appl. Crystallog.*, 1969, **2**, 65–71.
35 A. Ćirić, S. Stojadinović and M. D. Dramićanin, *Meas. Sci. Technol.*, 2019, **30**, 045001.
36 M. Lerch, H. Boysen and T. Hansen, *J. Phys. Chem. Solids*, 2001, **62**, 445–455.
37 A.M. Glazer, *Acta. Crystallogr. Sect. B Struct. Crystallogr. Cryst. Chem.,* 1972, **28**, 3384-3392
38 R. D. Shannon, *Acta Cryst.*, 1976, 751–767.
39 W. Mikenda and A. Preisinger, *J. Lumin* , 1981, **26**, 53–66.
40 H. Hua, J. Ueda, J. Xu, M. Back and S. Tanabe, *Inorg. Chem.*, 2021, acs.inorgchem.1c03074.
41 W. Ryba-Romanowski, S. Golab, G. Dominiak-Dzik, I. Sokolska and M. Berkowski, .
42 M. J. Weber and T. E. Varitimos, *J. Appl. Phys.*, 1971, **42**, 4996–5005.
43 P. I. Paulose, G. Jose, V. Thomas, N. V. Unnikrishnan and M. K. R. Warrier, *J. Phys. Chem. Solids*, 2003, **64**, 841–846.
44 J. Rocha, C. D. S. Brites and L. D. Carlos, *Chem. – Eur. J.*, 2016, **22**, 14782–14795.
45 T. P. van Swieten, A. Meijerink and F. T. Rabouw, *ACS Photonics*, 2022, **9**, 1366–1374.
46 A. Ćirić, Z. Ristić, Ž. Antić and M. D. Dramićanin, *Phys. B Condens. Matter*, 2022, **624**, 413454
47 L. Marciniak, A. Bednarkiewicz, J. Drabik, K. Trejgis and W. Strek, *Phys. Chem. Chem. Phys.*, 2017, **19**, 7343–7351.
48 K. Elzbieciak and L. Marciniak, *Front. Chem.*, 2018, **6**, 424
49 S. Wang, S. Westcott and W. Chen, *J. Phys. Chem. B*, 2002, **106**, 11203–11209.
50 A. Ćirić, J. Aleksić, T. Barudžija, Ž. Antić, V. Đorđević, M. Medić, J. Periša, I. Zeković, M. Mitrić and M. D. Dramićanin, *Nanomaterials*, 2020, **10**, 627.
51 V. A. Vlaskin, N. Janssen, J. van Rijssel, R. Beaulac and D. R. Gamelin, *Nano Lett.*, 2010, **10**, 3670–3674.
52 A. Ćirić, Z. Ristić, J. Periša, Ž. Antić and M. D. Dramićanin, *Ceram. Int.*, 2021, **47**, 27151–27156.
53 J. Ueda, M. Back, M. G. Brik, Y. Zhuang, M. Grinberg and S. Tanabe, *Opt. Mater.*, 2018, **85**, 510–516.

View Article Online
DOI: 10.1039/D2TC02011D

54 M. Back, J. Ueda, M. G. Brik, T. Lesniewki, M. Grinberg, S. Tanabe, *Acs Appl. Mater. Inter,* 2018, **10,** 41512-41524
55 Q. Wang, Z. Liang, J. Luo, Y. Yang, Z. Mu, X. Zhang, H. Dong and F. Wu, *Ceram. Int.*, 2020, **46**, 5008–5014.
56 A. Ćirić, Ł. Marciniak and M. D. Dramićanin, *J. Appl. Phys.*, 2022, **131**, 114501.
57 G. Gao, D. Busko, S. Kauffmann-Weiss, A. Turshatov, I. A. Howard and B. S. Richards, *J. Mater. Chem. C*, 2018, **6**, 4163–4170.
58 A. Ćirić, S. Stojadinović, Z. Ristić, I. Zeković, S. Kuzman, Ž. Antić and M. D. Dramićanin, *Adv. Mater. Technol.*, 2021, **6**, 2001201.
59 D. Yu, H. Li, D. Zhang, Q. Zhang, A. Meijerink and M. Suta, *Light Sci. Appl.*, 2021, **10**, 236.
60 A. M. Kaczmarek, M. Suta, H. Rijckaert, T. P. van Swieten, I. V. Driessche, M. K. Kaczmarek and A. Meijerink, *J. Mater. Chem. C*, 2021, **9**, 3589–3600.
61 R. G. Geitenbeek, P. T. Prins, W. Albrecht, A. van Blaaderen, B. M. Weckhuysen and A. Meijerink, *J. Phys. Chem. C*, 2017, **121**, 3503–3510.
62 P. V. Dos Santos, M. T. De Araujo, A. S. Gouveia-Neto, J. A. M. Neto and A. S. B. Sombra, *IEEE J. Quantum Electron.*, 1999, **35**, 395–399.